UC San Diego

UC San Diego Previously Published Works

Title

Water Mass Characteristics of the Antarctic Margins and the Production and Seasonality of Dense Shelf Water

Permalink

https://escholarship.org/uc/item/9fx3m2rx

Journal

Journal of Geophysical Research - Oceans, 124(12)

ISSN

2169-9275

Authors

Narayanan, Aditya
Gille, Sarah T
Mazloff, Matthew R
et al.

Publication Date

2019-12-01

DOI

10.1029/2018jc014907

Peer reviewed

eScholarship.org Powered by the California Digital Library
University of California

JGR Oceans

RESEARCH ARTICLE
10.1029/2018JC014907

Water Mass Characteristics of the Antarctic Margins and the Production and Seasonality of Dense Shelf Water

Aditya Narayanan[1], Sarah T. Gille[2], Matthew R. Mazloff[2], and K. Murali[1]

[1]Indian Institute of Technology Madras, Chennai, India, [2]Scripps Institution of Oceanography, University of California, San Diego, La Jolla, CA, USA

Abstract Conductivity-temperature-depth data from instrumented seals of the Marine Mammals Exploring Oceans from Pole to Pole program are analyzed to characterize the water masses and the seasonality of the marginal seas. Bottom temperatures are found to be in a cold regime in Dense Shelf Water (DSW) producing regions, identified in this study as the southern Weddell Sea, Cape Darnley, Prydz Bay, Adélie Coast, and the western Ross Sea. DSW occupies the bottom of the Weddell and Ross Sea continental shelves throughout the year: Production of DSW and vertical overturning occur only during the winter. In the other DSW producing regions, salinity is reduced more markedly during the summer. We identify the Princess Martha Coast, Leopold and Astrid Coast, and the Knox Coast as Low Salinity Shelf Water producing regions, where modified Circumpolar Deep Water (CDW) intrudes onto the continental shelf, reaching areas close to the ice shelves keeping the bottom temperatures in an intermediate regime. The Prince Harald Coast, the Amundsen Sea, and the Bellingshausen Sea experience more intense CDW intrusion, which keeps them in a warm regime year-round. CDW layer thicknesses correlate with the meridional winds over the shelf sea, and with the zonal winds at the slope, while DSW layer thicknesses correlate with the meridional winds over the shelf seas and the curl of the wind stress over the slope. Locations of DSW on the continental shelf coincide with an absence of warmer CDW near the ice shelves.

Key Points:
- Dense Shelf Water (DSW) production occurs in the Weddell Sea, Ross Sea, Cape Darnley, Prydz Bay, and the Adélie Coast
- Intermediate bottom temperature regimes occur in the Princess Martha Coast, Leopold and Astrid Coast, and the Knox Coast
- Locations of DSW on the continental shelf coincide with an absence of warmer Circumpolar Deep Water near the ice shelves

Supporting Information:
- Supporting Information S1

Correspondence to:
A. Narayanan,
adityarn@gmail.com;
adityarn@smail.iitm.ac.in

Citation:
Narayanan, A., Gille, S. T., Mazloff, M. R., & Murali, K. (2019). Water mass characteristics of the Antarctic margins and the production and seasonality of Dense Shelf Water. *Journal of Geophysical Research: Oceans, 124*. https://doi.org/10.1029/2018JC014907

Received 23 DEC 2018
Accepted 23 NOV 2019
Accepted article online 29 NOV 2019

©2019. American Geophysical Union. All Rights Reserved.

1. Introduction

Dense Shelf Water (DSW, with practical salinity $S > 34.5$, conservative temperature $-1.9\,°C \leq \theta \leq -1.8\,°C$, and neutral density $\gamma^n > 28.27$; Baines & Condie, 1998; Foster & Carmack, 1976; see Table 1) is produced in the marginal seas around Antarctica and plays an important role in ventilating the deep ocean. DSW participates in the meridional overturning circulation when it overflows the shelf seas into the deeper ocean, forming Antarctic Bottom Water (AABW, $\gamma^n > 28.27$; Orsi et al., 1999). DSW is hypothesized to function as a buffer, separating the ice shelves from intruding warm Circumpolar Deep Water (CDW, $S > 34.5, \theta \geq 0\,°C$), and is an important factor determining the stability of the ice shelves (Jacobs et al., 1992; Silvano et al., 2016).

The production of DSW depends on complex interactions between wind stress, sea ice, ice shelves, polynya formation, circulation in the shelf sea, and the water masses involved. Two major types of systems with DSW formation have been identified. The first of these is the classically identified wide-continental-shelf system (Foster & Carmack, 1976), which is found in regions such as the Weddell Sea and the Ross Sea. It involves the mixing of intruding CDW with Winter Water ($\theta < -1.7\,°C$ and $S < 34.5$) formed on the continental shelf and with shelf waters formed in coastal polynyas where brine discharge occurs due to sea ice production. The water column becomes completely destratified in the winter months allowing DSW to flood the continental shelf bottom. DSW further cools and slightly freshens due to the entrainment of Ice Shelf Water (ISW, $\theta < -1.9\,°C$), and it collects in the marginal sea basins, forming bottom waters such as Weddell Sea Bottom Water and Ross Sea Shelf Water (Jacobs et al., 1970). The residence time of bottom water in these wide continental shelf regions is estimated to be roughly 6 years (Gill, 1973; Jacobs et al., 1985), allowing sufficient time for the shelf water to collect at the sea bottom and become saltier. The western boundaries in the Ross and Weddell Seas allow for the western intensification of the overflows, which eventually exit the sea basins, forming bottom currents and downslope flows (Budillon et al., 2011; Foldvik et al., 2004).

The second system that supports DSW formation can occur in a number of narrow continental shelf regions around the continental margin, as identified by Baines and Condie (1998). These regions, such as the Adélie Land or Cape Darnley, lack the wide continental shelf, western boundary, and significant ice shelf-ocean interaction that contribute to bottom water formation in the Weddell and Ross Seas. Adélie Land bottom

Table 1
The Water Mass Definitions Used in This Study Are Listed Below

Water mass	Definition	Reference
DSW	$S > 34.5$, $-1.9\ °C \leq \theta \leq -1.8\ °C$, $\gamma^n > 28.27$	Williams et al. (2016)
High-density ISW	$S > 34.5$, $\theta < -1.9\ °C$, $\gamma^n > 28.27$	
ISW	$\theta < -1.9\ °C$	Schodlok et al. (2016)
LSSW	$34.3 < S < 34.4$, $-1.9\ °C \leq \theta \leq -1.5\ °C$	Schodlok et al. (2016)
mCDW	$-1.8\ °C < \theta < 0\ °C$, $28 < \gamma^n < 28.27$	Williams et al. (2016)
CDW	$S > 34.5$, $\theta \geq 0$	Jacobs et al. (1985)

Note. Schodlok et al. (2016) use a slightly different definition for LSSW with $34.3 < S < 34.35$, and Williams et al. (2016) do not have an upper temperature limit for mCDW. Figure S11 in the supporting information shows these water masses in θ-S space. High-density ISW, defined below, is used for identifying DSW producing regions (Table S2). Symbols used are conservative temperature (θ), practical salinity (S), and neutral density (γ^n).

water, identified by Rintoul (1998), forms via a mechanism involving especially strong offshore winds persistently keeping polynya regions open to produce DSW and Winter Water. Ohshima et al. (2013) described the formation of bottom water in the Cape Darnley polynya, a region of intense sea ice production averaging 8 m year^{-1} (Ohshima et al., 2016), which drives the formation of highly saline DSW in this region despite the narrowness of the continental shelf. This results in nearly complete destratification during winter months, which allows for strong vertical convection and for DSW to flood the bottom. Cape Darnley DSW contributes 0.65–1.5 Sv to AABW formation (Ohshima et al., 2013). This raises the possibility that other narrow-continental-shelf coastal polynya regions on the continental margin might also be AABW production zones.

DSW production depends on salt flux from sea ice production and is suppressed by freshwater influx. For example, regions such as the Amundsen Sea and the Sabrina Coast are active polynya regions with high sea ice production rates (Nihashi & Ohshima, 2015), but DSW production is suppressed by the meltwater influx in these regions (Petty et al., 2013; Silvano et al., 2018). Prydz Bay, with a relatively wide continental shelf along with a relatively large cold-cavity ice shelf, is a region of DSW formation. However, multiple studies have failed to observe DSW flowing off the Prydz Bay continental shelf (Meijers et al., 2010; Ohshima et al., 2013; Smith et al., 1984). Williams et al. (2016) found that the low salinity meltwater outflow at the western flank of the Amery Ice Shelf depresses the salinity of the DSW formed in the coastal polynya.

DSW has a direct influence on the basal melt rates and the stability of the ice shelf. Although DSW is cold, it can cause basal melting as it circulates beneath the ice shelves due to the pressure-dependent decrease of the freezing point at depth (Millero, 1978). However, DSW near the ice shelf buffers the ice shelf and ice sheets against the intrusion of warmer CDW, thereby reducing the net oceanic thermal forcing on the ice shelf-ice sheet systems. The DSW bottom water outflow becomes part of the westward flowing slope current maintained by the geostrophic balance at the Antarctic Slope Front. The balance is broken by bottom friction, and negative buoyancy drives the downslope transport of DSW, eventually forming AABW (Price & Baringer, 1994).

In regions that do not produce DSW, CDW more readily intrudes close to the ice shelves leading to high basal melt rates, as seen in the Amundsen Sea (Jacobs et al., 2011) and the Bellingshausen Sea (Jenkins & Jacobs, 2008). However, this is a complex problem, and the converse mechanism is also important: in regions experiencing CDW intrusion close to the ice shelves, the elevated basal melt rate leads to a freshwater influx that can suppress the formation of DSW. The suppression of DSW and vertical convection on the continental shelf further allows more CDW intrusion near the base of the ice shelves (Silvano et al., 2018). The Antarctic Circumpolar Current, the continental slope, and the Antarctic Slope Front present dynamical barriers to the intrusion of CDW onto the continental shelf, which is broken by mean (Rodriguez et al., 2016) and mesoscale processes that can drive CDW across these fronts (Gille et al., 2016; Heywood et al., 2014; Klinck & Dinniman, 2010). These processes include bottom Ekman transport (Dinniman & Klinck, 2004), eddies (Thompson et al., 2014), tides (Padman et al., 2009), mean transport (Stewart et al., 2018), cross-slope canyon steered flow (St-Laurent et al., 2013), and Kelvin wave-driven undercurrents (Chavanne et al., 2010; Webb et al., 2019). Petty et al. (2013) used mixed-layer models to show that atmospheric forcing plays an

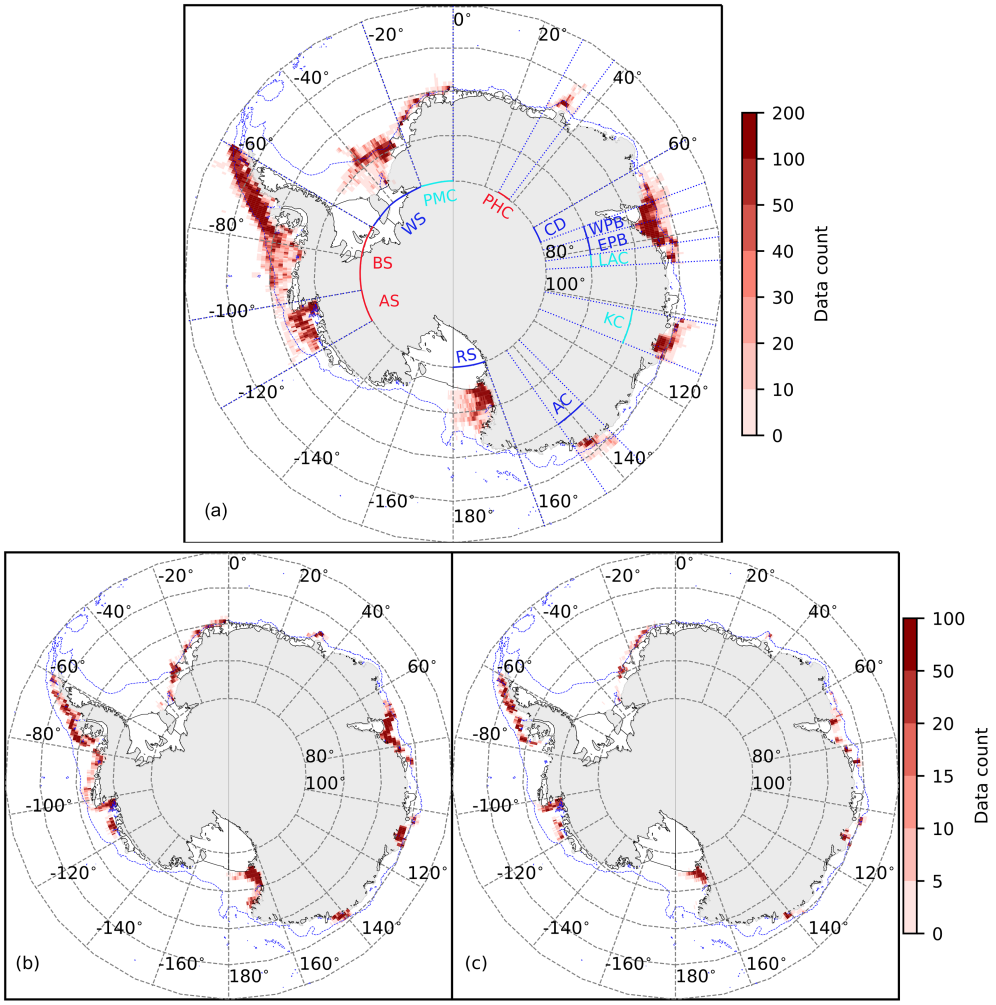

Figure 1. Number of profiles in the MEOP data set for years 2004 to 2017, aggregated in 0.5° × 0.5° cells for (a) all data used in this study, (b) near-ice-shelf areas during summer (December through May), and (c) near-ice-shelf areas during winter (June through November). The 1,000 m bathymetry contour is drawn to depict the continental shelf break. Regions depicted are the Weddell Sea (WS), Princess Martha Coast (PMC), Prince Harald Coast (PHC), Cape Darnley (CD), western Prydz Bay (WPB), eastern Prydz Bay (EPB), Leopold and Astrid Coast (LAC), Knox Coast (KC), Adélie Coast (AC), western Ross Sea (RS), Amundsen Sea (AS), and Bellingshausen Sea (BS). The longitudinal limits of these regions are marked by blue dashed lines. Annotations in the figure are color coded with dark blue for cold-regime regions, light blue for intermediate regions, and red for warm-regime regions. For more details on regions, refer to Table 2.

important role in determining CDW intrusion onto the continental shelf. Regions with strong easterlies over the continental slope have isopycnals that slope downward to the south, preventing the intrusion of CDW onto the continental shelf. In contrast, weak easterlies allow isopycnals to slope upward to the south, enabling CDW to shoal onto the shelf sea (Schmidtko et al., 2014; Stewart & Thompson, 2012).

In this study, we contrast the various marginal seas of the Antarctic, with a specific focus on the seasonality and regional distribution of DSW. We use data from the Marine Mammals Exploring Oceans Pole to Pole program (MEOP; Roquet et al., 2011) to identify the major water masses present on the continental shelf and immediately off-shelf. We study the seasonal variation of surface and bottom waters and estimate the monthly layer thicknesses of the major water masses. This enables us to categorize the marginal seas sampled by the MEOP program, distinguishing between those associated with (i) DSW production, (ii) modified CDW (mCDW, $-1.8\ ^\circ\mathrm{C} < \theta < 0\ ^\circ\mathrm{C}$, $28 < \gamma^n < 28.27$; Williams et al., 2016) intrusion and Low Salinity Shelf Water (LSSW, $34.3 < S < 34.4$, $-1.9\ ^\circ\mathrm{C} \leq \theta \leq -1.5\ ^\circ\mathrm{C}$; Schodlok et al., 2016) production, and (iii) no DSW but with intense mCDW and CDW intrusion. We analyze the interplay between DSW, mCDW, and CDW water masses on the continental shelf and show that where high water mass layer thicknesses of DSW

Table 2
Regions Sampled in the MEOP Data Set

Region	Code	Longitudes	Latitudes	Years (since 2000)	Regime	Width of shelf (km)
Southern Weddell Sea	WS	60°W to 20°W	≤75°S	7–9, 11, 14, 17	Cold	209
Princess Martha Coast	PMC	20°W to 0°	≤65°S	7–9, 11, 14–16	Intermediate	86
Prince Harald Coast	PHC	29°E to 37°E	≤65°S	4, 8, 11, 13–15, 17	Warm	161
Cape Darnley	CD	60°E to 70°E	≤65°S	4, 5, 7, 11–17	Cold	110
Western Prydz Bay	WPB	70°E to 75°E	≤65°S	5, 7, 9, 11–13, 15–17	Cold	191
Eastern Prydz Bay	EPB	75°E to 82°E	≤65°S	4–7, 9, 11, 12, 15–17	Cold	253
Leopold and Astrid Coast	LAC	82°E to 87°E	≤65°S	4, 9, 12, 13, 16	Intermediate	121
Knox Coast	KC	101°E to 112°E	≤60°S	4, 5, 7–17	Intermediate	125
Adélie Coast	AC	135°E to 145°E	≤60°S	5, 7–15, 17, 18	Cold	135
Western Ross Sea	RS	160°E to 180°E	≤72.5°S	10–12, 14, 16, 17	Cold	189
Amundsen Sea	AS	120°W to 100°W	≤70°S	5, 6, 8–10, 14	Warm	255
Bellingshausen Sea	BS	100°W to 60°W	≤60°S	5–10, 13–15	Warm	257

Note. Years with 100 or more profiles are listed. The regime in which each region lies is shown in column "Regime" (refer to sections 4 and 6).

are produced, there is a lack of CDW intrusion, and conversely, where CDW and mCDW intrusion is high, there is minimal DSW formation. Further, among the DSW producing regions, we distinguish seasonal and regional differences in DSW production, and we identify regions where meltwater suppresses the production of DSW.

2. MEOP Data Set

The marginal seas of the Southern Ocean have been chronically undersampled. However, the instrumented seal data set (Treasure et al., 2017) of the MEOP program provides a growing source of direct observations, with profiles often collected close to the ice shelves and during the winter. Profiles in the MEOP data set are spatially clustered and the sampling locations vary over time, depending on the migratory and foraging patterns of the instrumented mammals and the location of the colonies where the tagging was done. The profiles in this data set were collected over the period 2004 to 2017. Treasure et al. (2017) provide details on tagging locations, the foraging behavior of the seals, and the possible sampling biases arising from this.

Only profiles south of 60°S have been considered for this study. The sampling densities were higher in the southeastern Weddell Sea, Prydz Bay, Knox Coast, Adélie Coast, western Ross Sea, Amundsen Sea, and the Bellingshausen Sea (Figure 1). Figures 1b and 1c show the sampling locations in the near-ice-shelf regions (see section 3) during summer and winter respectively. Note that sampling is better in summer. A key limitation of this study is that the sampling locations differ across seasons, and this may have had an effect on our results, which is not quantified here. Further, the MEOP data set does not sample all the coastal polynyas, and this analysis is likely to have missed some important DSW-producing regions such as the eastern Ross Sea, the southwestern Weddell Sea, and a few coastal polynyas.

Roquet et al. (2011) described the delayed-mode calibration and statistical corrections that the CTD data collected by the tagged seals undergo before being released by the MEOP consortium. They estimate the instrument accuracy to be ±0.02 °C for temperature and ±0.1 for salinity without corrections. The delayed-mode calibration could be carried out either (i) in regions where ship based CTD measurements were available, improving accuracies to ±0.01 °C for temperature and ±0.03 for salinity, or (ii) in regions where the seals dived into the well-defined Lower CDW layer, improving accuracies to ±0.01 °C for temperature and ±0.02 for salinity. In other regions, the data undergo correction using a statistical cross-comparison technique. Corrections for the thermal mass error and instrument errors due to the miniaturization of the tags are also applied (Siegelman et al., 2019). In this study, we have only used data bearing a "good" quality flag, and we propagate the instrumental errors through all our calculations (see section 3). However, despite selecting for "good" data, manual quality inspection is also required based on our prior knowledge of the regions being studied. We found eight tags (tag serial numbers given in the supporting information text) that observed improbably high salinities ($35 < S < 35.5$) on the continental shelves of the Adélie Coast, Ross Sea, and the Weddell Sea, and data from these have been discarded from our analysis.

3. Methods

In this study, we focus on 12 major regions, as shown in Table 2. The distance is computed between each profile location and the closest point on the ice-shelf-edge or the grounding line, whichever is closer (GSHHG-2014; Wessel & Smith, 2014). Profiles that occur within a 75 km distance are considered as NIS (near-ice-shelf), and profiles that occur beyond are considered as DIS (distant-from-ice-shelf). Only profiles that occur over a seabed depth of 3,000 m or shallower are considered here to limit the data to the continental-shelf and continental-slope region. Throughout the text, we further divide these regions into two major groups (refer to Table S2). The first group consists of DSW-producing cold-regime regions where 5% or more of the data points in the NIS areas were consistent with DSW during the period from June to November. The second group of regions consists of non-DSW-producing intermediate-regime and warm-regime regions where less than 5% of data points in the NIS areas observed DSW during the June-to-November period. Note that dense ISW (with S> 34.5 and $\gamma^n > 28.27$ kg m^{-3}) is also considered as DSW to compute the percentage of DSW data points. Sections 4 and 6 provide more information on how we categorized the regions into the three different regimes.

Surface properties (not presented in the main text) are averaged over the upper 100 m of the water column and are referred to in the supporting information text as the surface box. The bottom box is defined as the portion of the water column below a cutoff depth, with the cutoff depth selected so that water in the bottom box can be characterized as having bottom properties. The property means are sensitive to the selection of bottom box depth cutoff. The root-mean-square error between the different choices are tabulated in Table S1 in the supporting information. In the main text, we use the bottom box defined to extend from 250 m depth to the sea floor, encompassing measurements collected at depths of 250 m depth or deeper. We also show temperature and salinity monthly means, with bottom boxes defined for depths below 375 or 500 m in Figures S1–S4 in the supporting information. For the cold-regime regions (Weddell Sea, Cape Darnley, Prydz Bay, Adélie Coast, and Ross Sea), deeper bottom boxes show slightly lower temperatures and slightly higher salinity. For the intermediate-regime regions (Princess Martha Coast, Leopold and Astrid Coast, and Knox Coast), deeper bottom boxes show a slight increase in mean temperature. In the warm-regime regions (Prince Harald Coast, Amundsen Sea, and the Bellingshausen Sea), the deeper bottom boxes show an increase in mean temperature. When we compare the results across regions, the results remain consistent regardless of whether we use 250, 375, or 500 m. In the main text, the decision to use bottom boxes extending from 250 m to the bottom is motivated by the need to have a consistent definition across all regions.

The error bars in the monthly mean surface box and bottom box property plots are defined as (1),

$$\epsilon = \sqrt{\overline{\mathrm{CTD}}_{\mathrm{error}}^2 + \alpha \frac{\sigma_{\mathrm{CTD}}{}^2}{\sqrt{N}}} \tag{1}$$

where N is the number of data points over which monthly mean is computed and $\alpha = 1.96$ is the factor of multiplication to obtain a 95% confidence limit on the standard error of the mean. For the surface box, σ denotes the standard deviation over all the data points in each month, whereas, for the bottom box, σ is computed over the entire year and not individually for each month. $\mathrm{CTD}_{\mathrm{error}}$ is the formal error of the corrected data as published by MEOP and represents a 95% confidence limit.

Water mass layer thicknesses were computed by dividing the water column in each region and in each month into vertical bins of 20 m and computing the fractional amount of each of the five water masses in each depth bin. The seal tags transmit compressed low-resolution data packets consisting of about 15 data points in the vertical, using a Broken Stick Method, for each profile (Photopoulou et al., 2015). We use these data points, without any interpolation, in our analysis. Since we include all the profiles available in the region and month being considered, most depth bins in the upper 500 to 700 m water column contain data (Figures S12 and S13). Some of the deeper bins, closer to the deepest depth of dive, may have no data and these bins are then discarded in the analysis. An important note here is that the low vertical resolution, and the spatiotemporal biases in sampling may have caused our analysis to miss some water masses.

Each individual data point in the depth and month bin was categorized as one of five water masses using the property ranges in Table 1 to obtain the fractional volume of each water mass in that bin. Finally, in each month, the fractional volumes of each water mass type were vertically integrated to determine the thickness of the water mass layer (i.e., the volume per unit area), with the assumption that water mass

properties are statistically homogeneous in each of the NIS and DIS regions. As a caveat, the water mass budgets computed here are representative only of the depth range and geographic coverage sampled by MEOP within each region. In each month and in each region, the 95% confidence interval was computed using the empirical bootstrap method (Efron & Tibshirani, 1994) by randomly resampling 1,000 times (with replacement) from each depth bin. In deeper depth bins, since the number of data points in the original sample is low to begin with, the resampling technique does not add any useful information regarding the confidence interval. However, in the intermediate and near-surface depth bins, the resampling technique provides a reasonable estimate of the confidence interval.

Water mass properties in different regions are compared using two strategies. First, the correlation coefficient between the average monthly DSW and CDW water mass layer thicknesses is computed. Second, for each region, the probability of either DSW or CDW being present is computed conditional on the presence or absence of CDW or DSW, using the climatological monthly mean water mass layer thicknesses. In this analysis, a water mass is considered to be present in a given month and region if its vertically integrated thickness exceeds the thickness of a single depth bin (i.e., 20 m). The presence or absence of a water mass is determined for each month in the climatology, and probabilities are aggregated separately for summer (from December to May) and winter (from June to November). The analysis includes both the NIS and DIS areas in each of the 12 regions. The 95% confidence interval was obtained by using the empirical bootstrap technique with 10,000 re-samplings for each seasonal bin.

Surface wind (10 m above the surface) data used in this study are from the ECMWF ERA-Interim monthly mean data set (Dee et al., 2011). The climatological mean of the monthly mean winds was computed over 2004–2017, the same period as the MEOP data set. Further, the spatial mean of the zonal wind and the curl of the wind stress at the continental slope within each region was used. However, the meridional wind was spatially averaged over the whole shelf sea (inshore of the 3,000 m isobath) of each region within the longitudinal and latitudinal limits as shown in Table 2, and the climatological monthly mean values were used. The continental slope was defined as the region with depths between 800 and 3,500 m where the gridded bathymetry (GEBCO 2014, 30 second arc bathymetry; Weatherall et al., 2015) gradient exceeds a value of 0.002. Appropriate latitudinal bounds for each region were used to prevent the high gradient regions near the coast from being selected. The width of the continental shelf was computed as the average of the shortest distance from the points on the slope to the ice shelf edge or the grounding line. The correlation coefficient between wind forcing and water mass layer thicknesses was computed using the monthly mean wind data and the monthly water mass layer thickness data. The zonal wind (U_{10}) is used as a proxy for the alongshore wind over the continental slope, and the meridional wind (V_{10}) is used to identify southerlies. The curl of wind stress was computed from gradients of the turbulent surface stress in the ERA-Interim data set.

4. Bottom Box Seasonality

Monthly mean properties for regions associated with DSW production (the southern Weddell Sea, Cape Darnley, Prydz Bay, Adélie Coast, and the western Ross Sea; see Table S2) are shown in Figure 2. In the Ross Sea (RS), and to some extent in the Weddell Sea (WS) and Prydz Bay (PB), DIS sampling occurred mostly on the continental shelf. In the other regions, DIS sampling occurred close to the shelf break and on the continental slope (see Figure S9), where the CDW layer elevates the bottom box temperatures. This is due to the larger width of WS, RS, and PB shelf seas compared to the other regions.

During the sea ice peak period from July to September, the bottom box temperatures are low in the WS-NIS (Figure 2a, mean temperature of $\bar{\theta} = -1.89 \pm 0.05$ °C), the RS-NIS (Figure 2i, $\bar{\theta} = -1.87 \pm 0.06$ °C), and the WPB-NIS (Figure 2c, $\bar{\theta} = -1.86 \pm 0.05$ °C). For the same period, in the deeper bottom box, from 500 m and below, WS-NIS temperatures are even lower (Figure S2a, $\bar{\theta} = -2.11 \pm 0.05$ °C) and are indicative of ice shelf meltwater outflow occurring at the Filchner Ice Shelf edge, which is consistent with the observations made by Foldvik et al. (1985) and Ryan et al. (2017).

The bottom box temperatures in the narrow-continental-shelf regions, during the period from January to March in the Cape Darnley-NIS (CD-NIS) (Figure 2b), have $\bar{\theta} = -1.69 \pm 0.12$ °C, from January to May in the Adélie Coast-NIS (AC-NIS) (Figure 2h), have $\bar{\theta} = -1.63 \pm 0.14$ °C, and from March to May in the East WS-NIS have $\bar{\theta} = -1.75 \pm 0.05$ °C. These temperatures are slightly elevated when compared to the other NIS regions, which all have wide continental shelves. The WS-NIS region includes both the wide

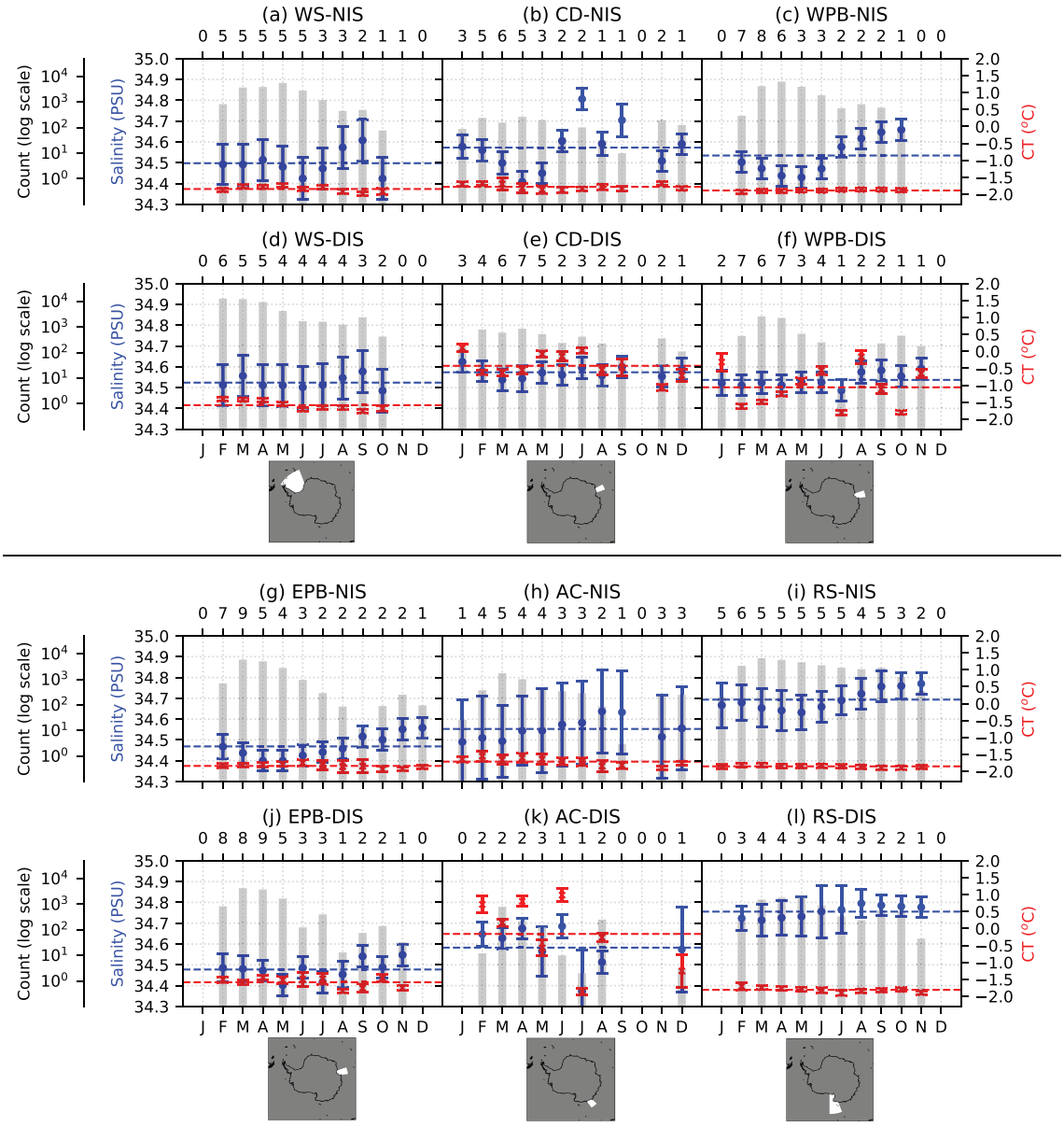

Figure 2. Monthly means of bottom (250 m and below) properties of Weddell Sea, Cape Darnley, west and east Prydz Bay, Adélie Coast, and the Ross Sea. Blue circles indicate salinity, while red crosses are for conservative temperature. Error bars are instrument error and standard error of mean (see section 3). Number of years during which each month was sampled is on upper X axis. Gray bars are sample size (plotted against extreme left Y axis). Annual mean salinity and conservative temperature are shown by the broken horizontal line in blue and red respectively. Inset maps indicate the longitudinal extent of each region.

continental-shelf area near the Filchner Ice Shelf, where bottom box temperatures remain low year-round (with $\bar{\theta} = -1.87 \pm 0.05$ °C in the NIS areas between 45°W and 30°W), and the narrow-continental-shelf area near the Stancomb Brunt Ice Shelf in the eastern Weddell Sea, where the slightly elevated bottom box temperatures occur (with $\bar{\theta} = -1.73 \pm 0.05$ °C in the NIS areas between 30°W and 20°W). However, CDW is not present in these regions, as seen in the TS plots in section 5, and the bottom box mean temperatures remain low in the deeper bottom boxes (Figures S1 and S2). In all the DSW-producing NIS regions, the mean bottom box temperatures remain below −1.5 °C, with no CDW present near the ice shelves (Figure 2). Hence, we categorize these regions as being in a cold regime.

While most regions show warmer bottom box temperatures in the DIS regions of Figure 2, the Weddell and Ross Seas (WS-DIS and RS-DIS) generally show low temperatures, with no CDW on the continental shelf. An exception occurs in August in the WS-DIS region (Figure S2d). However, the profiles containing CDW in the WS-DIS occurred close to the continental shelf break (Figure S5).

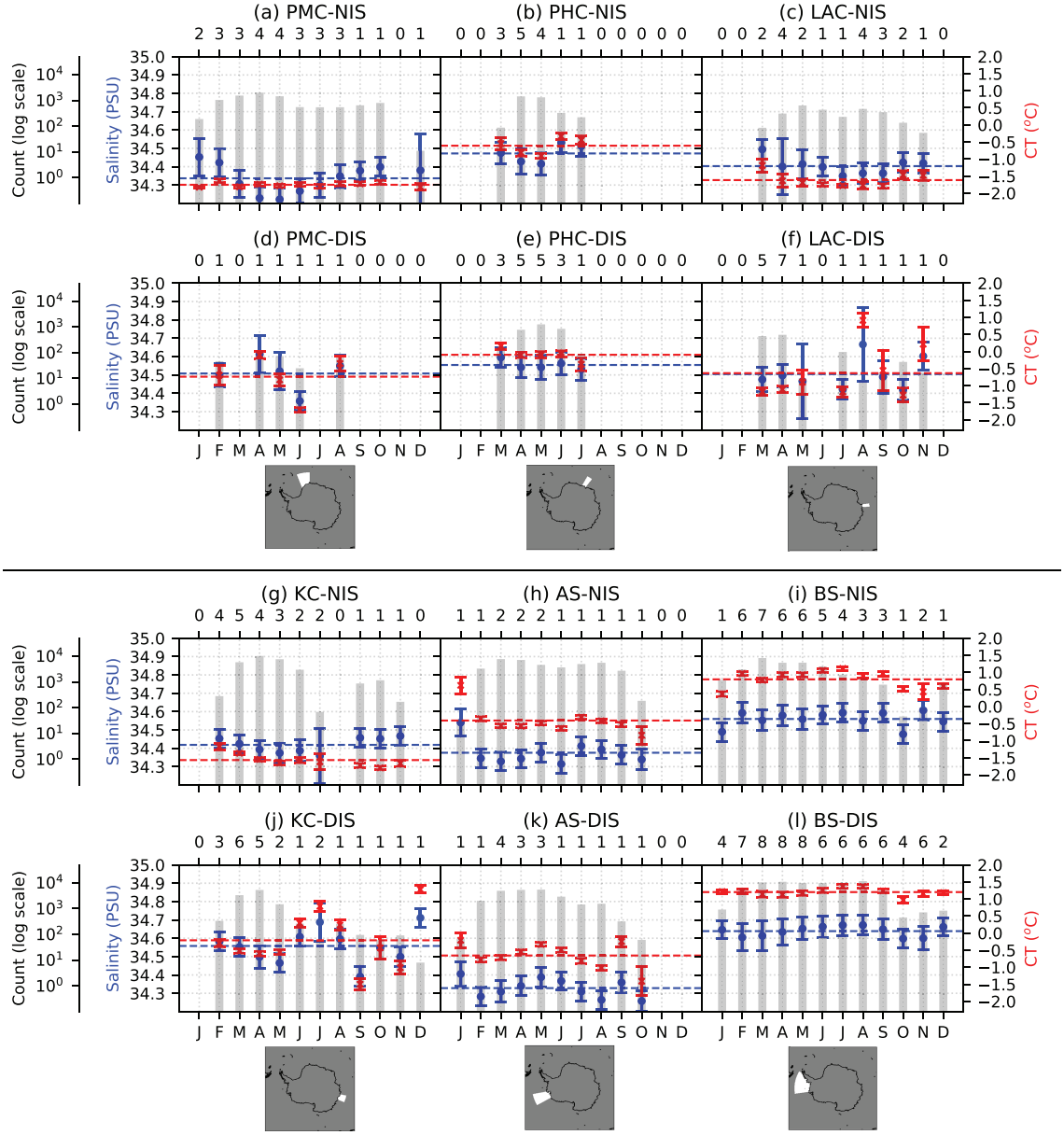

Figure 3. (a–l) Monthly means of bottom properties, 250 m and below for the Princess Martha Coast, Prince Harald Coast, Leopold and Astrid Coast, Knox Coast, Amundsen Sea, and Bellingshausen Sea. Blue circles indicate salinity, while red crosses are for conservative temperature. Error bars are instrument error and standard error of mean (see section 3). Number of years during which each month was sampled is on upper *X* axis. Gray bars are sample size (plotted against extreme left *Y* axis). Annual mean salinity and conservative temperature are shown by the broken horizontal line in blue and red respectively. Inset maps indicate the longitudinal extent of each region.

Mean salinities differ by region with highest year-round values in RS-NIS (Figure 2i) and RS-DIS (Figure 2l), where bottom box salinity always exceeds 34.5. WS-NIS (Figure 2a) and WS-DIS (Figure 2d) also have relatively stable year-round salinities, albeit with slightly lower values than in the RS-NIS and RS-DIS. In other NIS regions, salinities undergo seasonal and month-to-month variations. The largest variations occur in CD-NIS (Figure 2b) and WBP-NIS (Figure 2c), with both regions showing a marked decrease in summertime salinity. Both of these regions have comparable sea ice production rates (Nihashi & Ohshima, 2015); differences in timing and bottom box salinity maxima are consistent with the hypothesis that summer meltwater from the Amery Ice Shelf modulates DSW production in WPB-NIS (Williams et al., 2016), while in the Cape Darnley region, winter DSW production is the primary driver of salinity changes (Ohshima et al., 2013). The high salinities and low temperatures across all the NIS panels in Figure 2 are indicative of the presence of DSW.

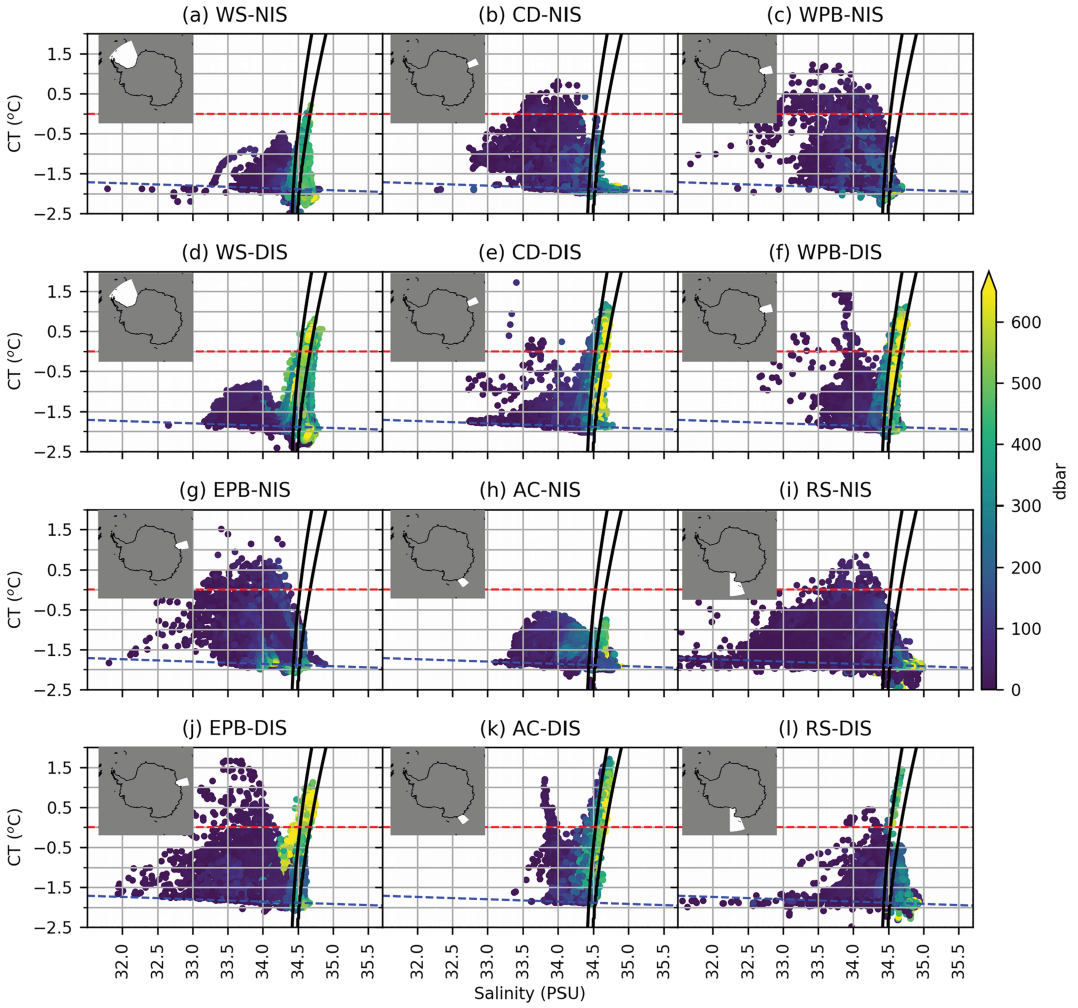

Figure 4. (a–l) Conservative temperature (CT) versus salinity plots with curves of $\gamma^n = 28.00, 28.27$ kg m^{-3} plotted. Surface freezing point is marked by the broken blue line at $\theta \approx -1.9$ °C, and the red broken line indicates $\theta = 0$ °C. Region codes are as in Table 2. Inset maps indicate the longitudinal extent of each region.

The monthly mean properties for regions not associated with DSW production (the Princess Martha Coast, Prince Harald Coast, Leopold and Astrid Coast, Knox Coast, Amundsen Sea, and the Bellingshausen Sea) are shown in Figure 3. The NIS bottom box temperatures are the highest in the Bellingshausen Sea (BS-NIS, Figure 3i) with $\bar{\theta} = 0.84 \pm 0.05$ °C, followed by the Amundsen Sea (AS-NIS, Figure 3h) with $\bar{\theta} = -0.5 \pm 0.05$ °C, and the Prince Harald Coast (PHC-NIS, Figure 3b) with $\bar{\theta} = -0.77 \pm 0.08$ °C. In the deeper bottom box (defined as depths below 500 m supporting information Figures S4i, S4h, and S4b), the mean conservative temperatures are all above 0 °C. Hence, we categorize these regions as being in a warm regime.

In the Princess Martha Coast ($\bar{\theta} = -1.74 \pm 0.05$ °C; Figure 3a, PMC-NIS), the Leopold and Astrid Coast ($\bar{\theta} = -1.7 \pm 0.1$ °C; Figure 3c, LAC-NIS), and the Knox Coast ($\bar{\theta} = -1.55 \pm 0.06$ °C; Figure 3g, KC-NIS), we find lower bottom box temperatures. We use the bottom box defined as depths below 500 m to show that the mean bottom box conservative temperature in the NIS regions of the Princess Martha Coast ($\bar{\theta} = -1.34 \pm 0.06$ °C; Figure S4a), the Leopold and Astrid Coast ($\bar{\theta} = -0.87 \pm 0.20$ °C; Figure S4c), and the Knox Coast ($\bar{\theta} = -1.47 \pm 0.05$ °C; Figure S4g) are higher ($\theta > -1.5$ °C) than the bottom box conservative temperatures of the DSW-producing cold-regime regions, while still being cooler than the mean temperatures of the warm-regime regions, placing them in an intermediate regime.

The high bottom box mean salinities in the warm-regime regions of PHC-NIS, AS-NIS, and BS-NIS are seen more prominently in the deeper bottom boxes in supporting information Figures S3 and S4, which, when coupled with the higher temperatures, are indicative of the presence of CDW in the NIS regions.

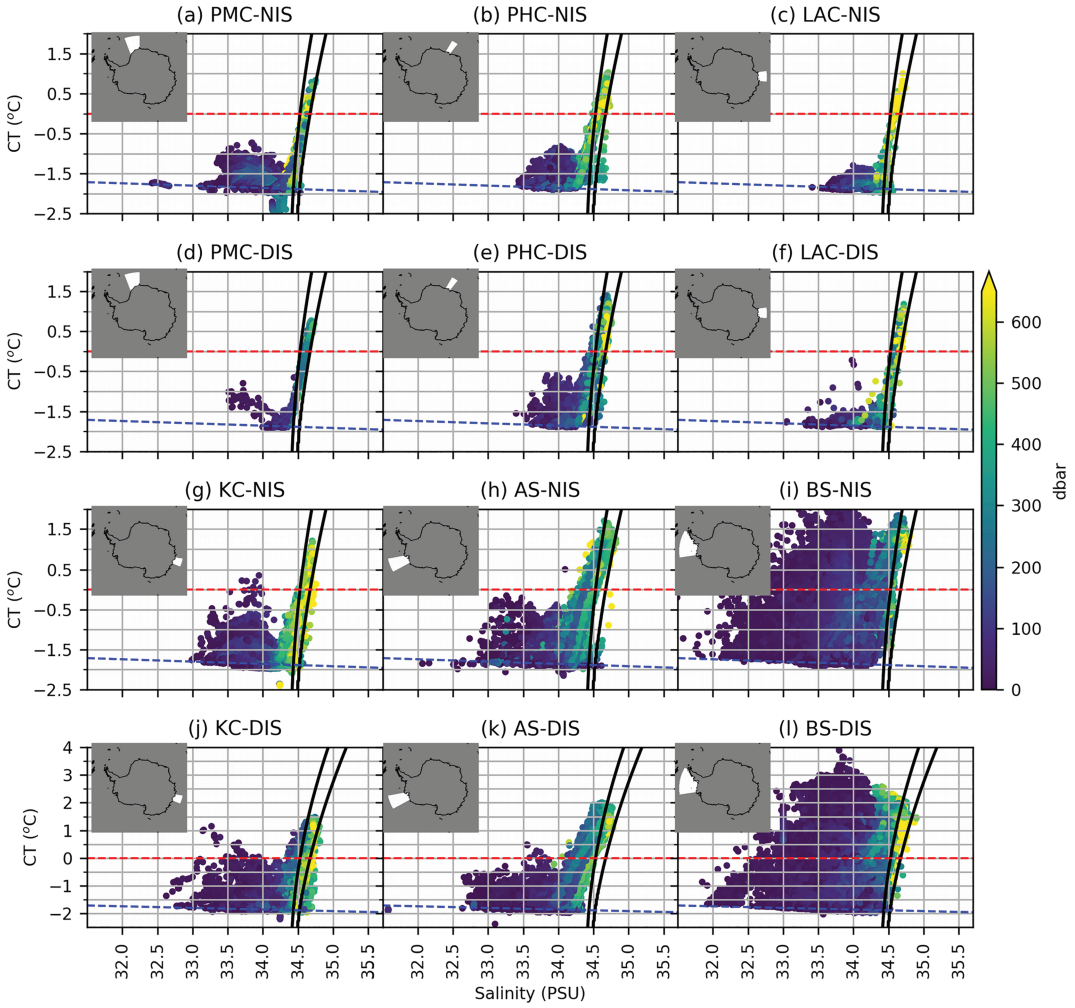

Figure 5. (a–l) Conservative temperature (CT) versus salinity plots with curves of $\gamma^n = 28.00, 28.27$ kg m^{-3} plotted. Surface freezing point is marked by the broken blue line at $\theta \approx -1.9$ °C, and the red broken line indicates $\theta = 0$ °C. Region codes are as in Table 2. Note that the CT scale changes for the bottom row. Inset maps indicate the longitudinal extent of each region.

In the intermediate-regime regions, the mean bottom box salinities are lower and are indicative of LSSW production.

5. Water Mass Characteristics

In this section, we use standard temperature-salinity (θ-S) plots to identify the major water masses in each region. We have grouped regions (see Table S2) where DSW is found in the near-ice-shelf (NIS) regions into Figure 4 and regions where DSW is not found in the NIS regions into Figure 5.

Across all the NIS panels of Figure 4, we observe low temperature DSW and mCDW but no CDW. In the DIS regions, which sample closer to the continental shelf break, we observe DSW along with both mCDW and CDW. However, the profiles detecting CDW occurred near the continental-shelf-break and slope region as can be seen in supporting information Figure S5.

As noted in section 1, the wide continental shelves and large cold-cavity ice shelves of the Weddell and Ross seas produce relatively less meltwater that can offset brine discharge from sea ice formation and are conducive to DSW production. WS-NIS primarily consists of profiles close to the Filchner and Stancomb Brunt Ice Shelf edges, while data for WS-DIS primarily consists of profiles on the continental shelf in the southeastern Weddell Sea (see Figure S9). The Weddell Sea has higher density DSW on the western continental shelf (with $S > 34.7$ and $\theta < -1.7$ °C; Foldvik et al., 1985), and this is not well sampled in the currently

available MEOP data set. The horizontal dashed lines in Figure 4 indicate the freezing point of seawater. In Figures 4a, 4d, 4i, and 4l, T-S points located below the dashed line correspond to cold ice shelf meltwater with high salinity in both the NIS and DIS regions of the Weddell Sea (WS) and Ross Sea (RS). We observe DSW with $S > 34.6$ in both the NIS and DIS regions of the WS and RS with the RS having the densest and highest salinity DSW. Orsi and Wiederwohl (2009) showed that the highest salinity DSW (with $S > 34.7$) is found in the western Ross Sea continental shelf, while the Central and Eastern Ross Sea continental shelves have lower salinity DSW.

Cold ISW of low salinity ($S < 34.5$) is observed in WPB-NIS (in Figure 4c), which is indicative of significant meltwater outflow from the Amery Ice Shelf. The DSW in Prydz Bay has lower salinity than in the NIS regions of the Weddell Sea, Ross Sea, Adélie Coast, and Cape Darnley, where we see higher salinity DSW forming. High salinity DSW is present in CD-NIS and ISW is absent (Figure 4b), as this region does not have a significant ice shelf.

CDW is present, in both the NIS and DIS regions, across all the panels in Figure 5. mCDW is warmer across all the NIS panels in the warm and intermediate-regime regions compared to the NIS regions of the cold-regime regions discussed earlier. The Princess Martha Coast, Leopold and Astrid Coast, and the Knox Coast have narrow continental shelves with CDW intruding close to the ice shelf edge. The Prince Harald Coast, the Amundsen Sea, and the Bellingshausen Sea have intense CDW intrusions onto the continental shelf near the ice shelves as seen in Figures 5b, 5h, and 5i, with the BS-NIS region being the only NIS region with no cold temperature (< -1.5 °C) mCDW. DSW is completely absent across all the panels of Figure 5. The monthly water mass layer thicknesses are presented later in section 6.

There exists a strong distinction between the water masses of the cold-regime regions of Figure 4 and those of the warm and intermediate-regime regions shown in Figure 5. In the cold-regime NIS regions, DSW is present and CDW water masses are absent. Conversely, in the warm and intermediate-regime NIS regions, DSW is largely absent, while warmer mCDW and CDW are seen to be intruding close to the ice shelves.

6. Water Mass Seasonal Layer Thicknesses

Monthly layer thicknesses of water masses for cold-regime regions are shown in Figure 6. Small quantities of mCDW are present during the summer months when DSW layer thicknesses are lower, and mCDW is mostly absent during the winter months when DSW layer thicknesses are higher in the wide continental shelf regions of WS-NIS (Figure 6a), WPB-NIS (Figure 6c), EPB-NIS (Figure 6g), RS-NIS (Figure 6i), and RS-DIS (Figure 6l). In the DIS areas of these wide-continental-shelf regions, mCDW is present almost throughout the year, except in RS-DIS, where small quantities (<100 m) are found. The RS-DIS region is unusual, because sampling occurred mostly on the continental shelf. In contrast, for the other DIS regions, sampling was distributed on the slope as well as near the continental shelf break, which resulted in a stronger distinction between NIS and DIS properties for regions other than the RS. Note that in some of the NIS regions, a fraction of ISW is higher in density and salinity (with $S > 34.5$ and $\gamma^n > 28.27$ kg m^{-3}; see Table 1) and is probably DSW that has mixed with meltwater. High-density ISW, as a fraction of total ISW, amounts to ~20% in the WS-NIS (with a maximum of ~70% in September), ~40% in WPB-NIS, ~40% in EPB-NIS, and ~90% in RS-NIS and RS-DIS combined.

The layer thicknesses of DSW peak in September in WS-NIS (Figure 6a, where ~70% of the ISW is cold DSW), WPB-NIS (Figure 6c), and RS-NIS (Figure 6i), occupying almost the whole water column of these shelf seas close to the ice shelves. The DSW layer thicknesses are low during the summer months and grow during the sea ice growth period. The monthly mCDW layer thicknesses in WPB-NIS (Figure 6c) and RS-NIS (Figure 6i) are low and are present predominantly during the summer months, when no CDW is present. Loose et al. (2009) observed greater concentrations of CDW and ISW in the eastern Ross Sea, which is not sampled in the MEOP data set. mCDW in WS-NIS (Figure 6a) and EPB-NIS (Figure 6g) is absent in September during the peak sea ice period. In the narrow-continental-shelf NIS regions of Cape Darnley (Figure 6b) and Adélie Coast (Figure 6h), mCDW is present almost throughout the year, while CDW is absent in these regions as well.

High monthly layer thicknesses of ISW are found in the WS-NIS (Figure 6a), WPB-NIS (Figure 6c), WS-DIS (Figure 6d), EPB-NIS (Figure 6g), RS-NIS (Figure 6i), and RS-DIS (Figure 6l). The mean bottom box salinity of ISW is 34.53 ± 0.10 in WS-NIS, 34.46 ± 0.05 in WPB-NIS, 34.74 ± 0.08 in RS-NIS, and 34.78 ± 0.12 in

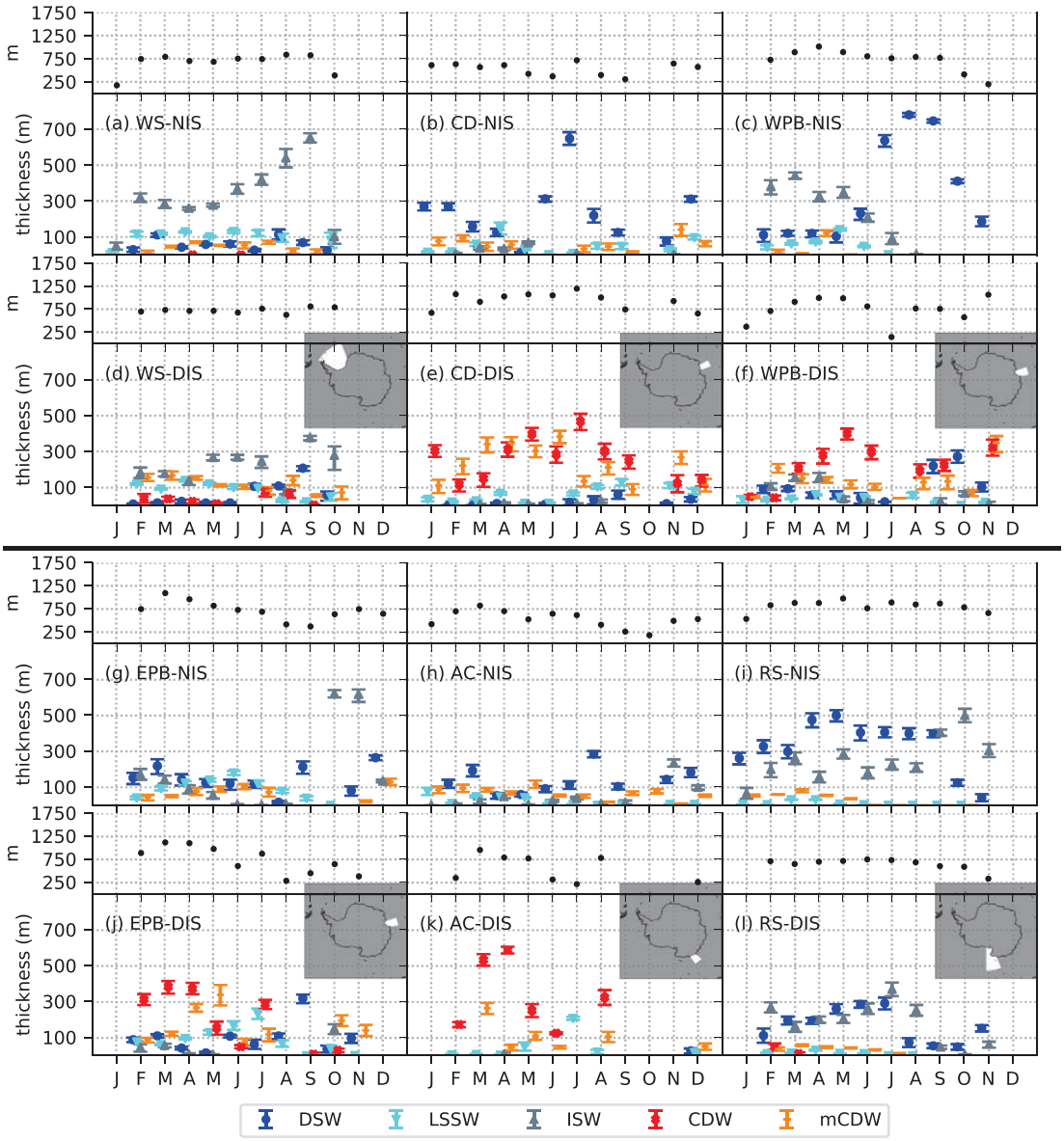

Figure 6. (a–l) Monthly water mass thickness for the DSW producing regions of Southern Weddell Sea, Cape Darnley, Western Prydz Bay, Eastern Prydz Bay, Adélie Coast, and western Ross Sea. Water masses are as defined in section 3. Black circular markers show the thickness of water column sampled in each month. Error bars denote the bootstrapped 95% CI. Inset maps indicate the longitudinal extent of each region.

RS-DIS, with the ISW in WPB-NIS and WS-NIS having lower bottom box salinities. Williams et al. (2016) showed that this ISW outflow from the Amery Ice Shelf in WPB-NIS is responsible for suppressing the formation of DSW and for lowering the mean salinity of the DSW formed in the Western Prydz Bay. Budillon et al. (2011) found that the DSW overflows in the western Ross Sea continental shelf through the Drygalski Trough were warmer and no ISW was observed, while the overflows in the central Ross Sea through the Glomar-Challenger Trough were cooler with ISW being present. In Cape Darnley and the Adélie Coast, we find no significant quantities of ISW.

The monthly water mass layer thicknesses for the intermediate and warm-regime regions are shown in Figure 7. Relatively high annually averaged monthly layer thicknesses of mCDW are found in the narrow continental shelf intermediate-regime NIS regions of Princess Martha Coast (105 ±26 m, Figure 7a), Leopold and Astrid Coast (108 ±24 m, Figure 7c), and the Knox Coast (321 ±36 m, Figure 7g), with the Knox Coast experiencing the highest quantity of mCDW intrusion among all the 12 NIS regions.

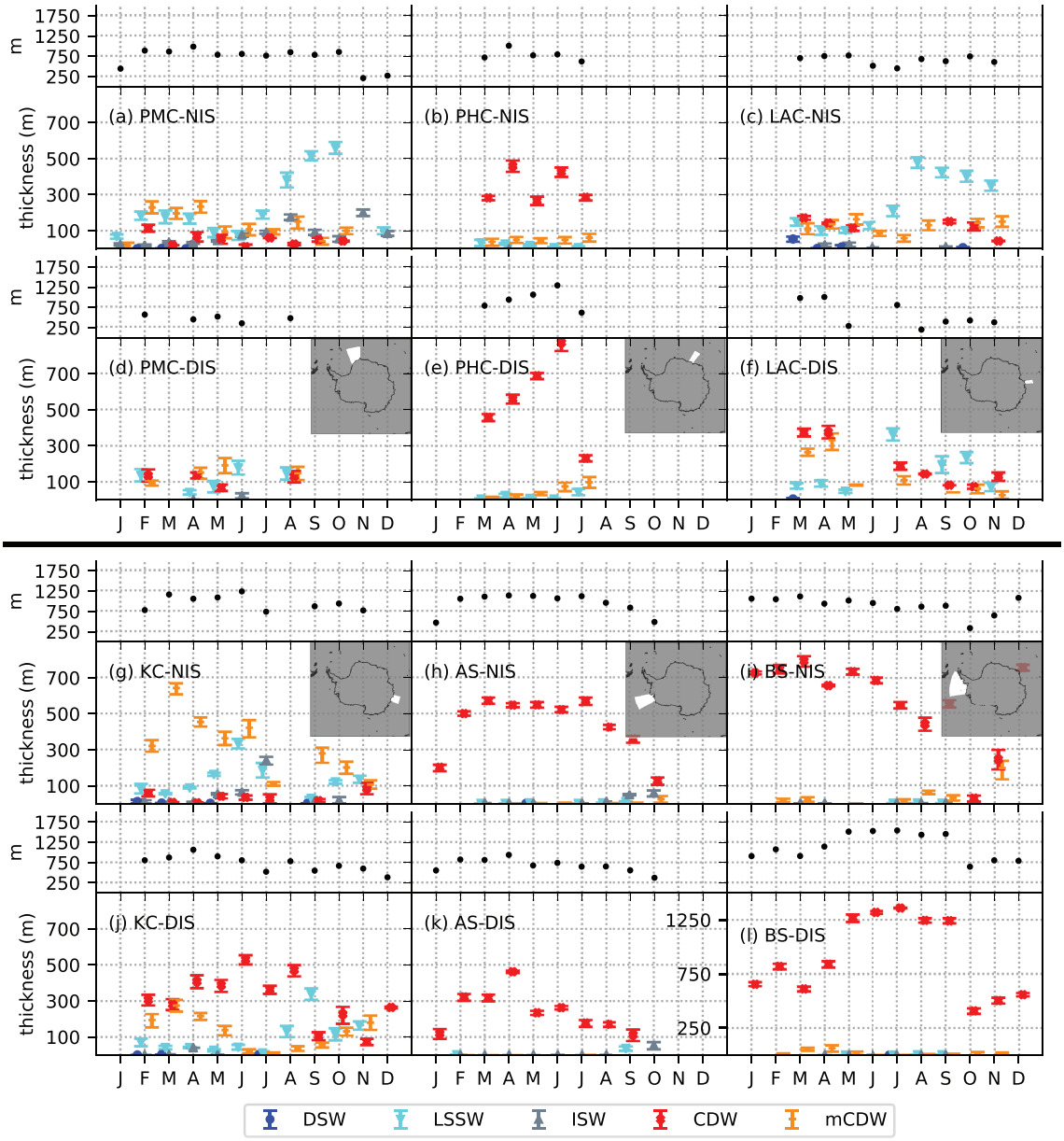

Figure 7. (a–l) Monthly water mass thickness for the non-DSW producing regions of Princess Martha Coast, Prince Harald Coast, Leopold and Astrid Coast, Knox Coast, Amundsen Sea, and Bellingshausen Sea. Water masses are as defined in section 3. Black circular markers show the thickness of water column sampled in each month. Note that the vertical scale changes for panel "(l) BS-DIS." Error bars denote the bootstrapped 95% CI. Inset maps indicate the longitudinal extent of each region.

The effect of the relatively higher quantity of mCDW in PMC-NIS, LAC-NIS, and KC-NIS is observed in the slightly elevated bottom box conservative temperatures that we see in these regions, as discussed in section 4. A classical mechanism of DSW formation involves the mixing of intruding mCDW with cold Winter Water and shelf waters produced in coastal polynyas to form DSW water masses (Foster & Carmack, 1976). Silvano et al. (2018) show that DSW production is insufficient to destratify the water column and cause deep convection in the Sabrina Coast (situated to the east of Knox Coast). In the absence of deep convection, without ventilating heat to the atmosphere, the intruding CDW can access the base of the ice shelves, where it elevates ice shelf melt rates. This, in turn, further suppresses DSW formation and results in the formation of LSSW. This hypothesis is consistent with our observations in the Princess Martha Coast, Leopold and Astrid Coast, and the Knox Coast where we find mCDW and LSSW year-round in the NIS regions. As shown in section 4, the bottom box temperatures in the intermediate-regime NIS regions are slightly warmer than

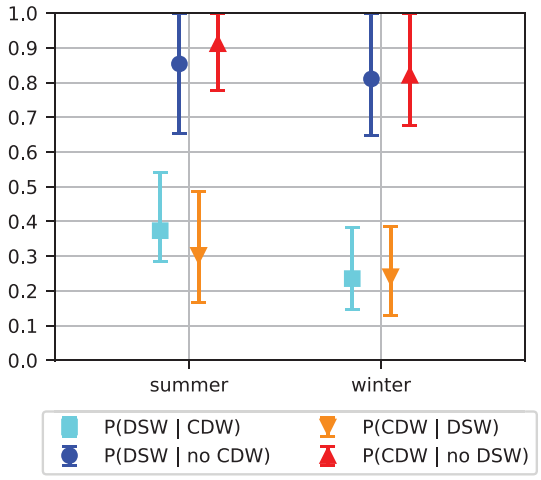

Figure 8. Summer (December to May) and wintertime (June to November) probabilities of the presence of DSW and CDW water masses conditional on each other's presence and absence across NIS and DIS areas of all 12 regions (refer to section 3). Error bars are the bootstrapped 95% confidence interval.

in the cold-regime NIS regions, while the bottom box salinities in the intermediate-regime regions are lower than what we find in the cold-regime NIS regions.

To put these results in context, we illustrate the effects of heightened intrusions of CDW and mCDW on the ice shelves by presenting melt rate estimates made by Rignot et al. (2013). They estimate the basal melt rates in the Totten Ice Shelf (east of the Knox Coast) to be 63.2 ± 4 Gt/year (10.5 ± 0.7 m/year), Shackleton Ice Shelf (east of LAC) to be 72.6 ± 15 Gt/year (2.8 ± 0.6 m/year), West Ice Shelf (in the LAC) to be 27.2 ± 10 Gt/year (1.7 ± 0.7 m/year), the Fimbul Ice Shelf (in the PMC) to be 23.5 ± 9 Gt/year (0.6 ± 0.2 m/year), and the Ekstrom Ice Shelf (in the PMC) to be 4.3 ± 2 Gt/year (0.6 ± 0.2 m/year). For comparison, the same study estimates the basal melt rates of ice shelves in the wider continental shelf seas of the Ross Sea and Weddell Sea, with the Ross East Ice Shelf basal melt rate at 49.1 ± 14 Gt/year (0.3 ± 0.1 m/year), Ross West Ice Shelf at −1.4 ± 20 Gt/year (0 ± 0.1 m/year), Filchner Ice Shelf (in the WS) at 41.9 ± 10 Gt/year (0.4 ± 0.1 m/year), and the Ronne Ice Shelf (in the RS) at 113.5 ± 35 Gt/year (0.3 ± 0.1 m/year). In the intermediate regime, narrow continental shelf regions of PMC, LAC, and KC, the meltwater inflow, which is similar in magnitude to the meltwater inflow in the wider continental shelves of the WS and RS, results in a thicker layer of fresh water at the surface that is sufficient to offset brine discharge from sea ice formation, and this is consistent with the suppression of DSW formation.

High annually averaged layer thicknesses of CDW were found in the warm-regime NIS regions of the Prince Harald Coast (PHC-NIS, 344 ± 24 m, Figure 7b), Amundsen Sea (AS-NIS, 437 ± 18 m, Figure 7h), and the Bellingshausen Sea (BS-NIS, 575 ± 26 m, Figure 7i). The MEOP data indicate no DSW or LSSW in these regions. In addition, mCDW is mostly absent in these regions.

These results suggest that in regions experiencing CDW intrusion onto the inner continental shelf, DSW is largely absent, and conversely, in regions where DSW is produced, CDW intrusion onto the inner continental-shelf is largely absent. We test this hypothesis by computing the probabilities of the presence or absence of DSW conditional on the presence or absence of CDW (and vice versa: CDW conditional on DSW) using the water mass layer thicknesses computed over both the NIS and DIS areas for all depth bins and all months. Figure 8 shows that the probability of finding DSW given the presence of CDW is low in both summer and winter. In contrast, the probability of finding DSW given no CDW presence in both summer and winter is high. Similarly, the probability of finding CDW given DSW presence in both summer and winter is low, and the probability of finding CDW given no DSW presence, in both summer and winter, is high. We find that DSW and CDW layer thicknesses are negatively correlated with a coefficient of −0.5 (CI= [−0.75to − 0.12]).

7. Wind Dynamics at the Shelf Break

The regime of each marginal sea ultimately depends upon the factors that drive DSW formation and the transport of CDW onto the continental shelf. Winds at the shelf break are important drivers of water mass exchange across the Antarctic Slope Front (Stewart & Thompson, 2012). As noted in section 3, three kinds of wind forcing are considered here: zonal winds ($-U_{slope}$), wind-stress curl ($-(\vec{\nabla} \times \vec{\tau})_{slope}$) spatially averaged over the continental slope, and meridional winds (V) averaged over the continental shelf within the latitudinal and longitudinal limits in Table 2. Easterly zonal winds drive a net southward Ekman transport of waters toward the coast resulting in coastal downwelling. This southward transport causes the CDW isopycnal surfaces from the open ocean to slope downward southward toward the slope front, restricting the CDW on-shelf transport (Spence et al., 2014). Southerly meridional winds blowing over the continental shelf advect sea ice away from the coastal polynya regions, increasing the sea ice production and export, and thus increasing the brine rejection leading to more DSW production (Abernathey et al., 2016). Finally, cyclonic wind stress curl $-(\vec{\nabla} \times \vec{\tau})_{slope}$ can drive an upwelling Ekman pump, which can transport the deeper warm CDW water masses onto the continental shelf (Rodriguez et al., 2016).

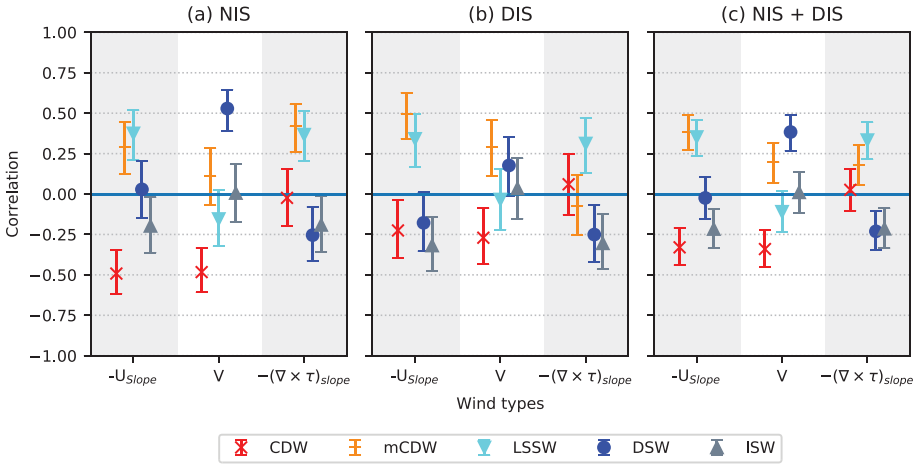

Figure 9. (a–c) Correlation between water mass layer thicknesses and the (i) climatological monthly mean of across slope easterlies ($-U_{slope}$) averaged at the continental slope of each region, (ii) climatological monthly mean southerlies spatially averaged over each region (V), and (iii) the climatological monthly mean of the cyclonic curl of the wind stress $-(\vec{\nabla} \times \vec{\tau})_{slope}$ spatially averaged at the slope of each region. Panels are divided into (a) NIS, (b) DIS, and (c) NIS+DIS areas of all the 12 regions. The error bars indicate the 95% CI for the correlation coefficient.

Before we present our results, we note here that our regression analysis may be missing causal relations by blending variability in time (monthly means) and space (across 12 regions). Another important caveat is that the wind data used here represent the climatological mean over the period 2004 to 2017. However, the water mass hydrography in each region is from a shorter time period (as shown in Table 2), with spatial and temporal sampling inhomogeneities that prevented us from weighting and selecting wind data from specific years to carry out the correlation. Further, the correlations we report here do not conclusively establish the mechanisms, which will instead require confirmation through more detailed process studies involving oceanographic observations and numerical models.

Figure 9 shows the correlation of climatological monthly mean water mass layer thicknesses with the climatological monthly mean winds. The layer thicknesses of CDW, in the NIS regions, correlate negatively with the easterlies at the slope ($r = -0.5$, CI = [−0.63 to −0.36]; Figure 9a) which is consistent with the hypothesis that the easterlies at the slope restrict the upwelling of CDW. In the DIS regions, CDW layer thicknesses correlate negatively with the easterlies (Figure 9b). However, rather counter-intuitively, the correlation is weaker here than in the NIS regions. We note here that CDW transport is affected by both mean and transient processes. The resulting interaction between intruding CDW and shelf water masses is complex, and a much more detailed analysis of models and observations is needed to explain this difference.

Further, in the NIS regions, CDW correlates negatively with the southerlies ($r = -0.51$, CI = [−0.63 to −40.36]), while DSW correlates positively ($r = 0.58$, CI = [0.45 to 0.69]) with the southerlies (Figure 9a). This is consistent with the hypothesis that the southerlies help advect sea ice northward, enabling DSW formation by enhancing the sea ice production rate in the coastal polynya, and thereby setting up deep convection.

In the NIS region (Figure 9a), DSW and ISW correlate negatively and mCDW and LSSW correlate positively with the cyclonic curl of the wind stress at the slope. In the DIS region (Figure 9b), we find that DSW and ISW correlate and LSSW anticorrelates with the cyclonic curl of the wind stress. Rodriguez et al. (2016) suggested that the time-mean component of the curl is a primary driver bringing CDW onto the continental shelf. (For a discussion of these results, please see section 8 below.) As a caveat, we note here that our water mass layer thickness analysis may underestimate the quantity of mCDW and CDW, as the deeper depth bins are poorly sampled in the MEOP data set.

8. Discussion and Conclusions

This study has used the MEOP database of hydrographic data from tagged seals to evaluate water mass properties in Antarctic marginal seas. We have categorized regions by their relative layer thicknesses of distinct water masses. The western Ross Sea, southern Weddell Sea, western Prydz Bay, eastern Prydz Bay, Cape Darnley, and the Adélie Coast are identified as DSW-producing regions, meaning that at least 5% of

the data points in the near-ice-shelf areas were consistent with DSW. These regions are also characterized by cold water at the base of the water column. The base of the water column here refers to the bottom box used in our analysis and extends up to the lowest depth of dive. However, since DSW are the densest water masses in these regions, they may extend beyond this depth for cases when the seals do not sample all the way to the seabed. Because the MEOP data are limited to places where instrumented elephant seals travel and locations where tagging took place, the data set does not sample some of the important DSW producing regions, such as the southwestern Weddell Sea and the eastern Ross Sea, and possibly some other narrow shelf polynya regions.

Throughout the year, DSW was observed at depth in the southern Weddell Sea and western Ross Sea, with the summer months showing a slight freshening. Summertime bottom box freshening and a reduction of DSW layer thickness are observed in western Prydz Bay. Our analysis confirms the hypothesis that the wide continental shelves in the WS, RS, and to some extent in Prydz Bay, allow sufficient residence time for the DSW to collect at the bottom and salinify. Other regions lack the large storage capacity, as they have narrower shelves, and we observe DSW bottom water only in the wintertime when DSW is produced at the surface, while in summertime the bottom water freshens with $S < 34.5$. No CDW intrusion was observed in the NIS region among these DSW producing regions.

The NIS areas of Princess Martha Coast, Leopold and Astrid Coast, and the Knox Coast fall into an intermediate regime. They are LSSW producing regions, where mCDW intrudes year-round. We find lower bottom salinities in these regions and slightly elevated bottom temperatures during the austral summer, with the Leopold and Astrid Coast having the most elevated bottom temperatures among all cold and intermediate-regime regions. The data confirm that the Prince Harald Coast, Amundsen Sea, and Bellingshausen Sea are in a warm-regime, with warm water supplied via intense CDW intrusion in the near ice shelf region.

The shelf sea water mass layer thicknesses of DSW and CDW correlate with the meridional winds over the shelf sea, and CDW layer thicknesses also correlate with the zonal winds at the slope. The presence of CDW in the DIS areas (close to the continental-shelf break) of cold-regime DSW-producing regions and the absence of CDW in the NIS areas of the same regions are consistent with the hypothesis (Silvano et al., 2016; Williams et al., 2016) that the presence of DSW on the continental shelf and the full water column convection occurring in these regions displaces intruding CDW water masses toward the surface, where they lose heat and mix with surface and shelf water masses and undergo transformation within the mixed layer (Marshall et al., 1999) to form cooler water masses (Abernathey et al., 2016). Further, our observation in the NIS areas that DSW weakly anticorrelates and mCDW correlates with the cyclonic curl of wind stress at the slope (Figure 9a) implies that upwelling processes contribute to conditions on the continental shelf, which is also consistent with this hypothesis.

Conditional correlations suggest a low probability of finding both DSW and CDW water masses present together. In the NIS regions the data suggest that DSW production buffers the ice shelves from the intruding mCDW and CDW. However, during the austral summer, DSW layer thicknesses fall, and mCDW is found intruding into the NIS regions. In the NIS regions absent of DSW, we observe large layer thicknesses of mCDW and CDW intruding close to the coastal polynya region. This mutually exclusive nature in the occurrence of DSW and CDW in the shelf seas is the underlying cause behind the sharp distinction in bottom sea temperatures of the marginal seas. The DSW-CDW interactions and the associated mechanisms need further investigation. As stated above, the results support the hypothesis that the presence of DSW and the processes enabling deep convection on the continental shelf, play an active role in dynamically blocking and transforming the intruding mCDW and CDW water masses before they can reach the ice shelves (Jacobs et al., 1992; Porter et al., 2019). However, there are other possible explanations for the observed distribution of bottom temperatures that cannot be ruled out from our results.

Schmidtko et al. (2014) have shown that the CDW layer is shoaling around the Southern Ocean, which could lead to increased coastward oceanic heat transport in the coming decades. The CDW observed at the continental-shelf break of the Weddell Sea at 500 m depth raises concerns, as CDW intrusion onto the continentel shelves of the Weddell Sea and the Ross Sea would have a serious warming effect on the ice shelves and on the ice sheets that they buffer (Hellmer et al., 2012). Moreover, Holland et al. (2019) show that future increases in anthropogenic greenhouse gas emissions can drive the formation of anomalous westerlies at the continental shelf break that can increase the shoreward heat transport. Our findings indicate that polynya

and wide-shelf seas of the Antarctic are important regions of DSW production and that DSW and CDW rarely coincide. Thus, for accurate projections of future glacial melt rates the complex interplay between winds, sea ice, and remote circulations in DSW formation must be further investigated.

Acknowledgments
We thank Laurie Padman and an anonymous reviewer for their helpful input. We are deeply grateful to the MEOP consortium for the valuable instrumented seal data set that made this study possible. It is available online (http://meop.net). Narayanan was supported by the Half Time Research Assistantship of IIT Madras and the support is gratefully acknowledged. Gille and Mazloff acknowledge support from the U.S. National Science Foundation (Grants NSF OCE-1658001, OCE-1924388, and PLR-1425989).

References

Abernathey, R. P., Cerovecki, I., Holland, P. R., Newsom, E., Mazloff, M., & Talley, L. D. (2016). Water-mass transformation by sea ice in the upper branch of the Southern Ocean overturning. *Nature Geoscience*, *9*(8), 596. https://doi.org/10.1038/ngeo2749

Baines, P. G., & Condie, S. (1998). Observations and modeling of Antarctic downslope flows: A review. *Ocean Ice and Atmosphere: Interactions at the Antarctic Continental Margin, Antarctic Research Series*, *75*, 29–49. https://doi.org/10.1029/AR075p0029

Budillon, G., Castagno, P., Aliani, S., Spezie, G., & Padman, L. (2011). Thermohaline variability and Antarctic bottom water formation at the Ross Sea shelf break. *Deep Sea Research Part I: Oceanographic Research Papers*, *58*(10), 1002–1018. https://doi.org/10.1016/j.dsr.2011.07.002

Chavanne, C. P., Heywood, K. J., Nicholls, K. W., & Fer, I. (2010). Observations of the Antarctic slope undercurrent in the southeastern Weddell Sea. *Geophysical Research Letters*, *37*, L13601. https://doi.org/10.1029/2010GL043603

Dee, D. P., Uppala, S. M., Simmons, A., Berrisford, P., Poli, P., Kobayashi, S., et al. (2011). The ERA-Interim reanalysis: Configuration and performance of the data assimilation system. *Quarterly Journal of the royal meteorological society*, *137*(656), 553–597. https://doi.org/10.1002/qj.828

Dinniman, M. S., & Klinck, J. M. (2004). A model study of circulation and cross-shelf exchange on the west Antarctic Peninsula continental shelf. *Deep Sea Research Part II: Topical Studies in Oceanography*, *51*(17-19), 2003–2022. https://doi.org/10.1016/j.dsr2.2004.07.030

Efron, B., & Tibshirani, R. J. (1994). *An introduction to the bootstrap*. New York: CRC press.

Foldvik, A., Gammelsrod, T., Osterhus, S., Fahrbach, E., Rohardt, G., Schroder, M., et al. (2004). Ice shelf water overflow and bottom water formation in the southern Weddell Sea. *Journal of Geophysical Research*, *109*, C02015. https://doi.org/10.1029/2003JC002008

Foldvik, A., Gammelsrød, T., & Tørresen, T. (1985). Circulation and water masses on the southern Weddell Sea shelf. *Oceanology of the Antarctic Continental Shelf*, *43*, 5–20. https://doi.org/10.1029/AR043p0005

Foster, T. D., & Carmack, E. C. (1976). Frontal zone mixing and Antarctic Bottom Water formation in the southern Weddell Sea. *Deep Sea Research and Oceanographic Abstracts*, *23*, 301–317. https://doi.org/10.1016/0011-7471(76)90872-X

Gill, A. (1973). Circulation and bottom water production in the Weddell Sea. *Deep Sea Research and Oceanographic Abstracts*, *20*, 111–140. https://doi.org/10.1016/0011-7471(73)90048-X

Gille, S. T., McKee, D. C., & Martinson, D. G. (2016). Temporal changes in the Antarctic Circumpolar Current: Implications for the Antarctic continental shelves. *Oceanography*, *29*(4), 96–105. https://doi.org/10.5670/oceanog.2016.102

Hellmer, H. H., Kauker, F., Timmermann, R., Determann, J., & Rae, J. (2012). Twenty-first-century warming of a large Antarctic ice-shelf cavity by a redirected coastal current. *Nature*, *485*(7397), 225–228. https://doi.org/10.1038/nature11064

Heywood, K. J., Schmidtko, S., Heuzé, C., Kaiser, J., Jickells, T. D., Queste, B. Y., et al. (2014). Ocean processes at the Antarctic continental slope. *Philosophical Transactions of the Royal Society A*, *372*(2019), 20130047. https://doi.org/10.1098/rsta.2013.0047

Holland, P. R., Bracegirdle, T. J., Dutrieux, P., Jenkins, A., & Steig, E. J. (2019). West Antarctic ice loss influenced by internal climate variability and anthropogenic forcing. *Nature Geoscience*, *12*(9), 718–724. https://doi.org/10.1038/s41561-019-0420-9

Jacobs, S. S., Amos, A. F., & Bruchhausen, P. M. (1970). Ross Sea oceanography and Antarctic Bottom Water formation. *Deep Sea Research and Oceanographic Abstracts*, *17*, 935–962. https://doi.org/10.1016/0011-7471(70)90046-X

Jacobs, S. S., Fairbanks, R. G., & Horibe, Y. (1985). *Origin and evolution of water masses near the Antarctic continental margin: Evidence from H218O/H216O ratios in seawater*. Washington: Wiley Online Library. https://doi.org/10.1029/AR043p0059

Jacobs, S. S., Helmer, H., Doake, C., Jenkins, A., & Frolich, R. (1992). Melting of ice shelves and the mass balance of Antarctica. *Journal of Glaciology*, *38*(130), 375–387. https://doi.org/10.3189/S0022143000002252

Jacobs, S. S., Jenkins, A., Giulivi, C. F., & Dutrieux, P. (2011). Stronger ocean circulation and increased melting under Pine Island Glacier ice shelf. *Nature Geoscience*, *4*(8), 519. https://doi.org/10.1038/ngeo1188

Jenkins, A., & Jacobs, S. (2008). Circulation and melting beneath George VI ice shelf, Antarctica. *Journal of Geophysical Research*, *113*, C04013. https://doi.org/10.1029/2007JC004449

Klinck, J., & Dinniman, M. (2010). Exchange across the shelf break at high southern latitudes. *Ocean Science*, *6*(2), 513–524. https://doi.org/10.5194/os-6-513-2010

Loose, B., Schlosser, P., Smethie, W., & Jacobs, S. (2009). An optimized estimate of glacial melt from the Ross Ice Shelf using noble gases, stable isotopes, and CFC transient tracers. *Journal of Geophysical Research*, *114*, C08007. https://doi.org/10.1029/2008JC005048

Marshall, J., Jamous, D., & Nilsson, J. (1999). Reconciling thermodynamic and dynamic methods of computation of water-mass transformation rates. *Deep Sea Research Part I: Oceanographic Research Papers*, *46*(4), 545–572. https://doi.org/10.1016/S0967-0637(98)00082-X

Meijers, A., Klocker, A., Bindoff, N., Williams, G., & Marsland, S. (2010). The circulation and water masses of the Antarctic shelf and continental slope between 30 and 80E. *Deep Sea Research Part II: Topical Studies in Oceanography*, *57*(9-10), 723–737. https://doi.org/10.1016/j.dsr2.2009.04.019

Millero, F. (1978). Freezing point of sea water. *Eighth report of the Joint Panel of Oceanographic Tables and Standards, Appendix*, *6*, 29–31.

Nihashi, S., & Ohshima, K. I. (2015). Circumpolar mapping of Antarctic coastal polynyas and landfast sea ice: Relationship and variability. *Journal of climate*, *28*(9), 3650–3670. https://doi.org/10.1175/JCLI-D-14-00369.1

Ohshima, K. I., Fukamachi, Y., Williams, G. D., Nihashi, S., Roquet, F., Kitade, Y., et al. (2013). Antarctic Bottom Water production by intense sea-ice formation in the Cape Darnley polynya. *Nature Geoscience*, *6*(3), 235–240. https://doi.org/10.1038/ngeo1738

Ohshima, K. I., Nihashi, S., & Iwamoto, K. (2016). Global view of sea-ice production in polynyas and its linkage to dense/bottom water formation. *Geoscience Letters*, *3*(1), 13. https://doi.org/10.1186/s40562-016-0045-4

Orsi, A. H., Johnson, G. C., & Bullister, J. L. (1999). Circulation, mixing, and production of Antarctic Bottom Water. *Progress in Oceanography*, *43*(1), 55–109. https://doi.org/10.1016/S0079-6611(99)00004-X

Orsi, A. H., & Wiederwohl, C. L. (2009). A recount of Ross Sea waters. *Deep Sea Research Part II: Topical Studies in Oceanography*, *56*(13-14), 778–795. https://doi.org/10.1016/j.dsr2.2008.10.033

Padman, L., Howard, S. L., Orsi, A. H., & Muench, R. D. (2009). Tides of the northwestern Ross Sea and their impact on dense outflows of Antarctic Bottom Water. *Deep Sea Research Part II: Topical Studies in Oceanography*, *56*(13-14), 818–834. https://doi.org/10.1016/j.dsr2.2008.10.026

Petty, A. A., Feltham, D. L., & Holland, P. R. (2013). Impact of atmospheric forcing on Antarctic continental shelf water masses. *Journal of Physical Oceanography*, *43*(5), 920–940. https://doi.org/10.1175/JPO-D-12-0172.1

Photopoulou, T., Lovell, P., Fedak, M. A., Thomas, L., & Matthiopoulos, J. (2015). Efficient abstracting of dive profiles using a broken-stick model. *Methods in Ecology and Evolution*, *6*(3), 278–288. https://doi.org/10.1111/2041-210X.12328

Porter, D. F., Springer, S. R., Padman, L., Fricker, H. A., Tinto, K. J., Riser, S. C., et al. (2019). Evolution of the seasonal surface mixed layer of the Ross Sea, Antarctica, observed with autonomous profiling floats. *Journal of Geophysical Research: Oceans*, *124*, 4934–4953. https://doi.org/10.1029/2018JC014683

Price, J. F., & Baringer, M. O. (1994). Outflows and deep water production by marginal seas. *Progress in Oceanography*, *33*(3), 161–200. https://doi.org/10.1016/0079-6611(94)90027-2

Rignot, E., Jacobs, S., Mouginot, J., & Scheuchl, B. (2013). Ice-shelf melting around Antarctica. *Science*, *341*(6143), 266–270. https://doi.org/10.1126/science.1235798

Rintoul, S. R. (1998). On the origin and influence of Adélie Land Bottom Water, *Ocean, ice, and atmosphere: Interactions at the Antarctic continental margin* (pp. 151–171). Washington, DC: AGU. https://doi.org/10.1029/AR075p0151

Rodriguez, A. R., Mazloff, M. R., & Gille, S. T. (2016). An oceanic heat transport pathway to the Amundsen Sea Embayment. *Journal of Geophysical Research: Oceans*, *121*, 3337–3349. https://doi.org/10.1002/2015JC011402

Roquet, F., Charrassin, J.-B., Marchand, S., Boehme, L., Fedak, M., Reverdin, G., & Guinet, C. (2011). Delayed-mode calibration of hydrographic data obtained from animal-borne satellite relay data loggers. *Journal of Atmospheric and Oceanic Technology*, *28*(6), 787–801. https://doi.org/10.1175/2010JTECHO801.1

Ryan, S., Hattermann, T., Darelius, E., & Schröder, M. (2017). Seasonal cycle of hydrography on the eastern shelf of the Filchner Trough, Weddell Sea, Antarctica. *Journal of Geophysical Research: Oceans*, *122*, 6437–6453. https://doi.org/10.1002/2017JC012916

Schmidtko, S., Heywood, K. J., Thompson, A. F., & Aoki, S. (2014). Multidecadal warming of Antarctic waters. *Science*, *346*(6214), 1227–1231.

Schodlok, M., Menemenlis, D., & Rignot, E. (2016). Ice shelf basal melt rates around Antarctica from simulations and observations. *Journal of Geophysical Research: Oceans*, *121*, 1085–1109. https://doi.org/10.1002/2015JC011117

Siegelman, L., Roquet, F., Mensah, V., Rivière, P., Pauthenet, E., Picard, B., & Guinet, C. (2019). Correction and accuracy of high and low resolution CTD data from animal borne instruments. *Journal of Atmospheric and Oceanic Technology*, *36*(5), 745–760. https://doi.org/10.1175/JTECH-D-18-0170.1

Silvano, A., Rintoul, S. R., & Herraiz-Borreguero, L. (2016). Ocean-ice shelf interaction in East Antarctica. *Oceanography*, *29*(4), 130–143.

Silvano, A., Rintoul, S. R., Peña-Molino, B., Hobbs, W. R., van Wijk, E., Aoki, S., et al. (2018). Freshening by glacial meltwater enhances melting of ice shelves and reduces formation of Antarctic Bottom Water. *Science Advances*, *4*(4), eaap9467. https://doi.org/10.1126/sciadv.aap9467

Smith, N. R., Zhaoqian, D., Kerry, K. R., & Wright, S. (1984). Water masses and circulation in the region of Prydz Bay, Antarctica. *Deep Sea Research Part A. Oceanographic Research Papers*, *31*(9), 1121–1147. https://doi.org/10.1016/0198-0149(84)90016-5

Spence, P., Griffies, S. M., England, M. H., Hogg, A. M., Saenko, O. A., & Jourdain, N. C. (2014). Rapid subsurface warming and circulation changes of Antarctic coastal waters by poleward shifting winds. *Geophysical Research Letters*, *41*, 4601–4610. https://doi.org/10.1002/2014GL060613

St-Laurent, P., Klinck, J. M., & Dinniman, M. S. (2013). On the role of coastal troughs in the circulation of warm Circumpolar Deep Water on Antarctic shelves. *Journal of Physical Oceanography*, *43*(1), 51–64. https://doi.org/10.1175/JPO-D-11-0237.1

Stewart, A. L., Klocker, A., & Menemenlis, D. (2018). Circum-Antarctic shoreward heat transport derived from an eddy-and tide-resolving simulation. *Geophysical Research Letters*, *45*, 834–845. https://doi.org/10.1002/2017GL075677

Stewart, A. L., & Thompson, A. F. (2012). Sensitivity of the ocean's deep overturning circulation to easterly Antarctic winds. *Geophysical Research Letters*, *39*, L18604. https://doi.org/10.1029/2012GL053099

Thompson, A. F., Heywood, K. J., Schmidtko, S., & Stewart, A. L. (2014). Eddy transport as a key component of the Antarctic overturning circulation. *Nature Geoscience*, *7*(12), 879. https://doi.org/10.1038/ngeo2289

Treasure, A., Roquet, F., Ansorge, I. J., Bester, M. N., Boehme, L., Bornemann, H., et al. (2017). Marine mammals exploring the oceans pole to pole: A review of the MEOP consortium. *Oceanography*, *30*, 132–138.

Weatherall, P., Marks, K. M., Jakobsson, M., Schmitt, T., Tani, S., Arndt, J. E., et al. (2015). A new digital bathymetric model of the world's oceans. *Earth and Space Science*, *2*(8), 331–345. https://doi.org/10.1002/2015EA000107

Webb, D., Holmes, R., Spence, P., & England, M. (2019). Barotropic Kelvin wave-induced bottom boundary layer warming along the West Antarctic Peninsula. *Journal of Geophysical Research: Oceans*, *124*, 1595–1615. https://doi.org/10.1029/2018JC014227

Wessel, P., & Smith, W. (2014). Shoreline boundary between Antarctic grounding line and the ocean, 2014 (High-resolution). (v. 2.3.3). http://purl.stanford.edu/pg150hg9699

Williams, G., Herraiz-Borreguero, L., Roquet, F., Tamura, T., Ohshima, K., Fukamachi, Y., et al. (2016). The suppression of Antarctic bottom water formation by melting ice shelves in Prydz Bay. *Nature communications*, *7*, 12577. https://doi.org/10.1038/ncomms12577